An Investigation into the Dynamics of Chalcopyrite Bioleaching

Athanasios Kotsiopoulos, Geoffrey S. Hansford, and Randhir Rawatlal
Dept. of Chemical Engineering, University of Cape Town, Rondebosch 7701, South Africa

DOI 10.1002/aic.12183
Published online January 20, 2010 in Wiley Online Library (wileyonlinelibrary.com).

A study was undertaken to investigate the dynamics of chalcopyrite bioleaching. The analysis revealed significant dynamics features because the chemical leaching rate of chalcopyrite does not vary monotonically with solution redox potential but undergoes a maximum followed by a minimum as potential increases. The analysis does account for reaction passivation, an effect that has consistently been reported in the literature. The existence and stability of steady states were determined as functions of the solution redox potential, reactor temperature, and biomass concentration. It was found that the rate of bioleaching increased with temperature at lower overall solution potentials with competitive rates observed at high ferric/ferrous ion ratios. Both high and low overall bioleaching rates were observed with increasing biomass concentration, indicating an upper concentration limit before passivation. These results indicate that the frequently observed inhibiting rates may simply be artifacts of the system dynamics rather than due to physical phenomena. © 2010 American Institute of Chemical Engineers *AIChE J,* 56: 2650–2661, 2010

Keywords: reaction kinetics, reactor analysis, mathematical modeling

Introduction

The indirect mechanism of bioleaching involves the ferric iron attack of the sulfide mineral at the surface liberating ferrous ions into solution (Eq. 1). Through microbial oxidation, the ferrous ions are converted back to the ferric form (Eq. 2). The constant generation of ferrous ions and regeneration of ferric ions resulting from the chemical and microbial oxidation reactions, respectively, create an environment, which is autocatalyzed and sustained by the presence of microorganisms.

$$CuFeS_2 + 4Fe^{3+} \rightarrow Cu^{2+} + 5Fe^{2+} + 2S^0 \quad (1)$$

$$4Fe^{2+} + O_2 + 4H^+ \rightarrow 4Fe^{3+} + 2H_2O. \quad (2)$$

Correspondence concerning this article should be addressed to R. Rawatlal at randhir.rawatlal@uct.ac.za.

Although bioleaching of metal sulfides has been successfully applied for the recovery of gold, copper, and other base metals, the rate of dissolution of chalcopyrite is very slow in both chemical and microbial leaching environments.

Low rates of chalcopyrite leaching have been attributed to the formation of a passivating layer thought to evolve from both iron- and sulfur-containing precipitates, hindering the transfer of ions to and from the chalcopyrite surface.[1] Several conflicting reports suggest that an increase in ferrous ion concentration may or may not increase the rate of chalcopyrite leaching.[2–4] Although chalcopyrite bioleaching at elevated temperatures is known to increase the production rate, the reduced cellular rigidity at these temperatures makes the cell structure susceptible to mechanical stress, resulting in reduced rates of extraction.[5–9] Low rates of dissolution have also been attributed to oxygen transfer limitations.[8–11]

These kinetic considerations were the fundamental building blocks of the model developed by Kotsiopoulos et al.[12] to predict the overall performance of continuous-flow bioleach reactor systems. Although the model was shown to

accurately predict plant operation, it was found that because of the nonlinearity of the reaction rate expressions, a rigorous dynamics analysis of bioleaching kinetics is required to optimize and evaluate input conditions for safe operation and maximizing the production rate.

In biological systems, a sustained dynamic equilibrium is reached when there is balance between microbial growth and substrate availability. This indicates that system steady state will only exist if there is sufficient substrate for microbial growth. In contrast to the proposals by previous researchers, which only account for low bioleaching rates due to inhibiting phenomena such as a passivating layer, shear stresses, and oxygen transfer limitations, we wish to investigate whether the dynamics of the kinetics of chalcopyrite bioleaching are a direct result of these unfavorable rates.

Model Development

The mechanism of bioleaching is a set of reactions whereby iron is exchanged between the ferric and ferrous ion form via chemical leaching and microbial oxidation reactions (Eqs. 1 and 2, respectively). At steady state, this exchange defines the rate and redox potential at which the bioleach reactor will operate.[13] In bioleaching, the solution redox potential is related to the ferric to ferrous ion ratio ($[Fe^{3+}]/[Fe^{2+}]$) via the Nernst equation. The ferrous ions formed from chemical leaching (Eq. 1) decreases the solution redox potential, whereas microbial oxidation increases the solution redox potential by the regeneration of ferric ions. The overall solution redox potential therefore only increases if the rate of microbial oxidation is greater than the rate of chemical leaching.

At steady state, the rate at which ferrous ions are liberated from the mineral sulfide particle surface equals the rate at which microbial ferrous ions are consumed in solution. Whether or not this point is stable is largely dependent on the concentration of the biomass and hence on the microbial activity, as well as the concentration of the sulfide mineral.[14] The chemical leaching and microbial oxidation kinetics must therefore be related to the process conditions as a function of the ferric/ferrous ion ratio to determine the steady state(s).

For the sake of clarity, we first develop a dynamics analysis for the simpler case of pyrite bioleaching. For most mineral sulfide ores, the chemical leach kinetics are represented as the ferric to ferrous ion ratio to the *n*th order (Eq. 3)

$$-r''_{MS} = k\left(\frac{C_{Fe^{3+}}}{C_{Fe^{2+}}}\right)^{n}, \tag{3}$$

where r''_{MS} is the intrinsic rate (mol m^{-2} s^{-1}), k the intrinsic rate constant (mol m^{-2} s^{-1}), and n can be approximated to be 0.5.[15]

As such, the chemical leaching rate increases monotonically with an increase in solution redox potential. The rate has a slow initial increase at low potentials because of ferrous ion inhibition and gradually increases at higher potentials when more ferric ions are available for reaction (Figure 1).

It should be noted that the intrinsic rate r''_{MS} (mol m^{-2} s^{-1}) is a surface area–based rate, and therefore, the overall rate of leaching in the reactor is obtained by multiplying the intrinsic rate by the total particle specific surface area A^p (m^2 m^{-3}). In reality, the particle surface area may change with time because of reaction. The particle surface area can be considered as constant in flow reactor systems where the mean particle residence time is low with respect to the leaching rate time scale. For simplicity, the total specific surface area available for reaction A^p (m^2 m^{-3}), in the following case studies, is lumped together with the intrinsic leaching rate constant and is assumed constant. More generally, however, the approach of segregation outlined by Kotsiopoulos et al.[12] should be adopted to account for the varying particle sizes and hence surface area.

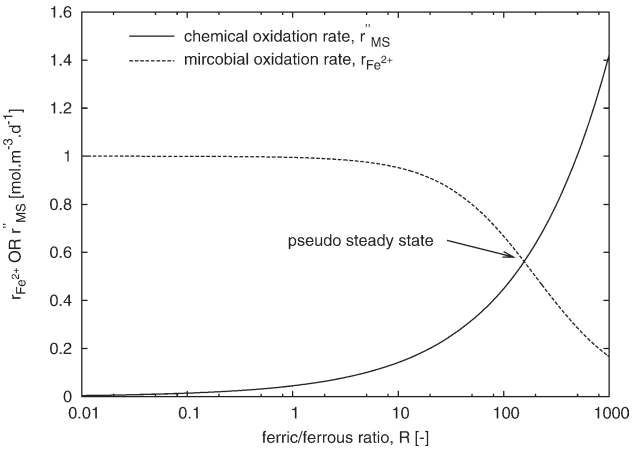

Figure 1. Stable steady state indicated by the point of intersection between the microbial oxidation and chemical leaching rate curves.

The microbial oxidation rate equation is based on Michaelis-Menten/Monod type kinetics and developed by Hansford[16] (Eq. 4).

$$-r_{Fe^{2+}} = \frac{C_X q^{max}_{Fe^{2+}}}{1 + K\frac{C_{Fe^{3+}}}{C_{Fe^{2+}}}}, \tag{4}$$

where $q^{max}_{Fe^{2+}}$ (mol Fe^{2+} mol^{-1} carbon s^{-1}) is the maximum microbial specific ferrous iron utilization rate, K the inhibition constant, and C_X, $C_{Fe^{3+}}$, and $C_{Fe^{2+}}$ are the concentrations of the biomass (mol carbon m^{-3}), ferric, and ferrous ions, respectively (mol m^{-3}).

From the microbial kinetics, it is apparent that the microbial oxidation rate is directly proportional to the concentration of the biomass in solution and is a function of the redox potential. Microbial kinetics of this type therefore accounts for the effect of ferric ion inhibition, indicating that the rate of microbial growth decreases with increasing solution potential (Figure 1).

According to Breed and Hansford,[13] when a batch system is at equilibrium, the rate of chemical ferrous ion production equals the rate of microbial ferrous ion consumption (Eq. 5).

$$-r^{micro}_{Fe^{2+}} = r^{chem}_{Fe^{2+}}. \tag{5}$$

However, in the bioleach process, which is inherently multiphase, ions are constantly liberated from the mineral

into solution. This forces a never-ending increase of the total concentration of iron in solution, and therefore a steady state with respect to the absolute concentration of any ionic species is never actually attained. The point of intersection of the chemical leaching (Eq. 3) and microbial oxidation (Eq. 4) rate curves is shown in Figure 1. It must be noted that, in a batch reactor, these curves, and hence this point of intersection, are changing with time. As the time scale of this move is much less than the reaction time scale, this intersection point, according to Breed and Hansford,[13] is effectively a pseudo-steady state.

Model Dynamics

According to Eq. 3, the rate of iron turnover in the system increases with the increase in the ferric/ferrous iron ratio ($R = [Fe^{3+}]/[Fe^{2+}]$). The rate at which the solution redox potential varies is therefore the change in the concentration of ferric ions relative to the change in concentration of the ferrous ions in the multistep mechanism (Eq. 6)

$$\frac{dR}{dt} = \frac{C_{Fe^{2+}} \cdot \frac{dC_{Fe^{3+}}}{dt} - C_{Fe^{3+}} \cdot \frac{dC_{Fe^{2+}}}{dt}}{C^2_{Fe^{2+}}}. \quad (6)$$

As the denominator $C^2_{Fe^{2+}}$ is always positive, $C_{Fe^{2+}} \cdot \frac{dC_{Fe^{3+}}}{dt} = C_{Fe^{3+}} \cdot \frac{dC_{Fe^{2+}}}{dt}$ at steady state with respect to R.

During batch operation, the change in ferric and ferrous ions with time is the rate at which the ions are produced and consumed. Generally, these material balances can be written as (Eqs. 7 and 8):

$$\frac{dC_{Fe^{3+}}}{dt} = -\alpha r_{MS} + r_{Fe^{2+}} \quad (7)$$

$$\frac{dC_{Fe^{2+}}}{dt} = \beta r_{MS} - r_{Fe^{2+}}, \quad (8)$$

where α and β are the stoichiometric coefficients of the ferric and ferrous ions in solution according to the chemical leaching reaction, respectively. In the case of pyrite bioleaching, α and β are the numerical values 14 and 15, respectively, whereas for chalcopyrite bioleaching $\alpha = 4$ and $\beta = 5$ according to Eqs. 1 and 2, respectively.

By substituting Eqs. 7 and 8 into Eq. 6, and noting that the redox potential R is the ratio of the ferric to ferrous ions in solution, Eq. 6 can be rewritten in the form of Eq. 9

$$\frac{dR}{dt} = \frac{(R+1) \cdot r_{Fe^{2+}} - (\beta R + \alpha) \cdot r_{MS}}{C_{Fe^{2+}}}. \quad (9)$$

As the denominator on the right-hand side is always positive, the system will reach a steady state with respect to R at the condition given by Eq. 10.

$$(R+1) \cdot r_{Fe^{2+}} = (\beta R + \alpha) \cdot r_{MS}. \quad (10)$$

At any point, when the rate of microbial oxidation exceeds the rate of chemical leaching or vice versa, the solution redox potential either increases or decreases, respectively, until the system is at steady state.

Dynamics of Pyrite Bioleaching

Acid ferric sulfate solutions formed from the microbial oxidation of pyrite play an important role in the commercial recovery of, for example, copper from metal sulfide ores. Higher rates of pyrite oxidation would therefore increase rates of leaching.[17]

As bioleaching involves the transfer of ions from the solid particle phase to the surrounding solution phase, the total iron concentration is never constant. In the chemical leaching of pyrite represented by Eq. 11, for example, $\alpha = 14$, ferric ions, which are already in solution, are converted to the ferrous form, as well as liberating an additional Fe center from the ore particle as ferrous, hence $\beta = 15$.

$$FeS_2 + 14Fe^{3+} + 8H_2O \rightarrow 15Fe^{2+} + 2SO_4^{2-} + 16H^+. \quad (11)$$

Therefore, the analogy proposed by Breed and Hansford[13] that the rate of the microbial and chemical oxidation rates is equal at steady state (Eq. 5) only applies for the rate of production and consumption of the ferrous ions and does not hold true for the ferric ions. As the ferric ion concentration is not steady, and because of the existence of a thermodynamic equilibrium between the two ionic forms, the concentration of ferrous ions will also tend to change with time. The only possible steady state is therefore with respect to the ferric/ferrous ion ratio R as predicted by Eq. 9.

The point of intersection according to the generally reported pseudo-steady state (Eq. 5, Figures 2a, b) and the pseudo-steady state rigorously derived in this article (Eq. 9, Figures 2c, d) are shown for a pyrite ore (Eq. 10) using kinetic parameters outlined in Table 1. Clearly, the assumption that pseudo-steady state for the ionic species equates to pseudo-steady state for redox potential is not valid. For this reason, previous attempts at dynamics analysis were not capable of accurately modeling the observed passivation effects. We now develop this analysis for the case of chalcopyrite rather than pyrite bioleaching.

Dynamics of Chalcopyrite Bioleaching

For most mineral sulfide ores, a single stable steady state exists (Figure 1). However, according to the studies reported by Kametani and Aoki,[18] the chemical leaching rate of chalcopyrite does not vary monotonically with R, but goes through a maximum followed by a minimum as solution potential increases. On the other hand, the microbial action does vary monotonically with R. As such, there may exist as many as three steady states.

Hiroyoshi et al.[2] proposed that the chemical leaching of chalcopyrite includes a reduction step in which the chalcopyrite is converted to Cu_2S. The chalcocite intermediate is then rapidly oxidized releasing Cu^{2+} ions into solution (Eq. 12). Thereafter, $Cu_{1.2}S$ undergoes ferric ion oxidation, at a lower rate, further releasing Cu^{2+} ions into solution according to Eq. 13.[15]

$$Cu_2S + 1.6Fe^{3+} \rightarrow Cu_{1.2}S + 0.8Cu^{2+} + 1.6Fe^{2+} \quad (12)$$

$$Cu_{1.2}S + 4Fe^{3+} \rightarrow 1.2Cu^{2+} + 2.4Fe^{2+} + S^0. \quad (13)$$

On the basis of the mechanism proposed by Hiroyoshi et al.,[19] Petersen and Dixon[15] suggested that the rate

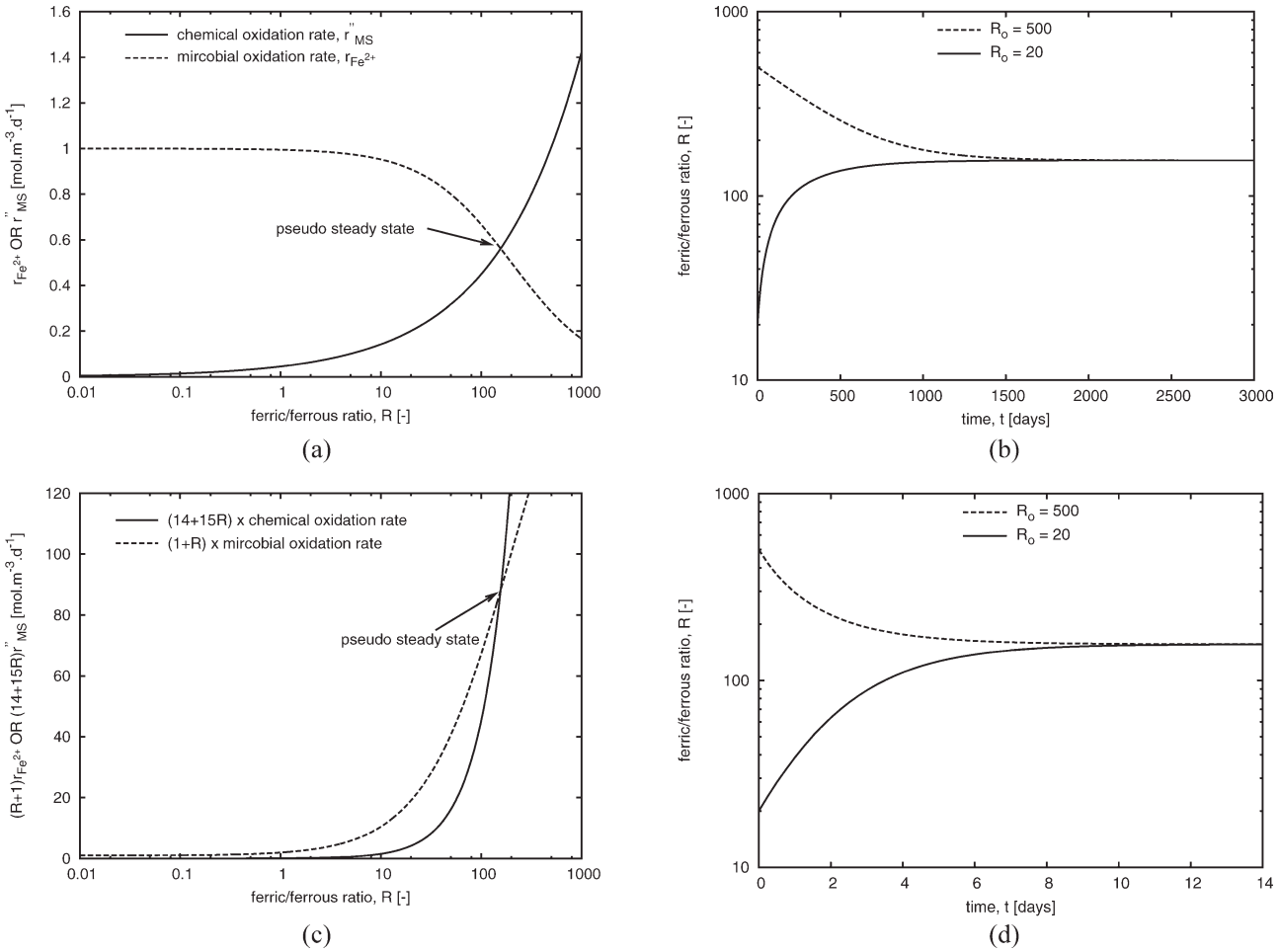

Figure 2. Operating point for most mineral sulfide ores. A single stable steady state exists at the point of intersection ($R = [Fe^{3+}]/[Fe^{2+}]$).

(a) and (b) correspond to rate and transient plots, respectively, using the generally accepted method in Eq. 5; (c) and (d) are rate and transient plots, respectively, determined using Eq. 9, derived in this study.

expression for these two reactions, each producing Cu^{2+}, could be lumped into the single empirical formula given in Eq. 14. Figure 3 illustrates the contributions from each term, representing the contribution from each of the two reactions that give one overall nonmonotonic curve.

$$r_{\text{cpy}} = g_{\text{py}} \cdot f(X_{\text{cpy}}) \cdot R^{0.5}\left[A\exp\left(-\frac{R}{R_{\text{crit}}}\right) + B\left(1-\exp\left(-\frac{R}{R_{\text{crit}}}\right)\right)\right], \quad (14)$$

where g_{py} is the mineral grade, which is the fraction of mineral ore content in the ore body, $f(X_{\text{cpy}})$ is the topological term, which accounts for the change in the mineral reacting surface, and A and B are the temperature-dependent kinetic rate constants.

As with pyrite, the dynamics analysis on chalcopyrite was performed using Eqs. 9 and 10. Figure 4a shows a plot of the microbial oxidation and chemical leaching rate functions $(R + 1)r_{\text{Fe}^{2+}}$ and $(5R + 4)r_{\text{cpy}}$, respectively. Points of intersection X, Y, and Z in Figure 4a indicate steady-state points at the corresponding redox potential R, while the corresponding reaction rates are determined from the chemical leaching rate curve at the corresponding redox potentials R shown in the accompanying Figure 4b.

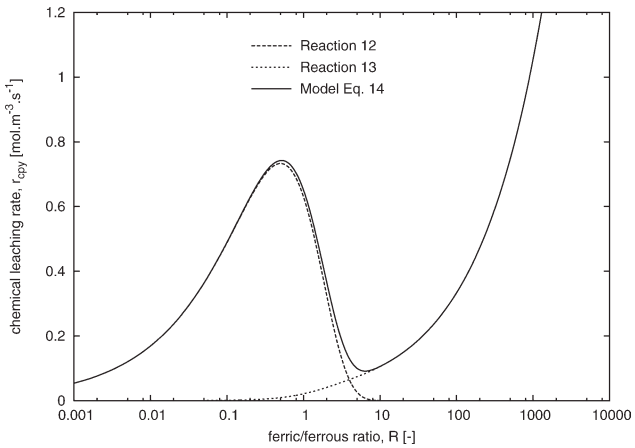

Figure 3. Graphical representation of the empirical chalcopyrite leaching rate proposed by Petersen and Dixon.[15]

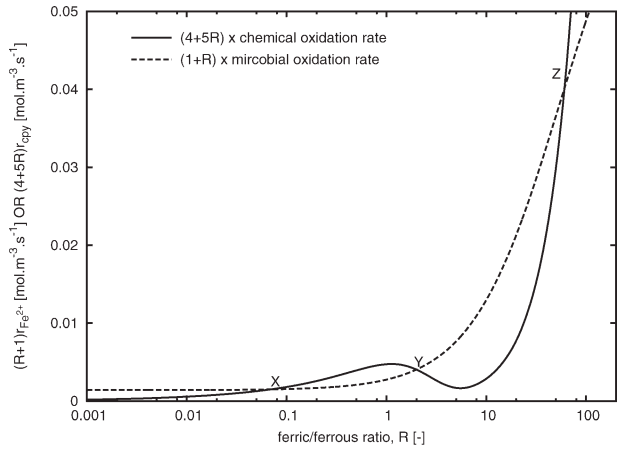

(a)

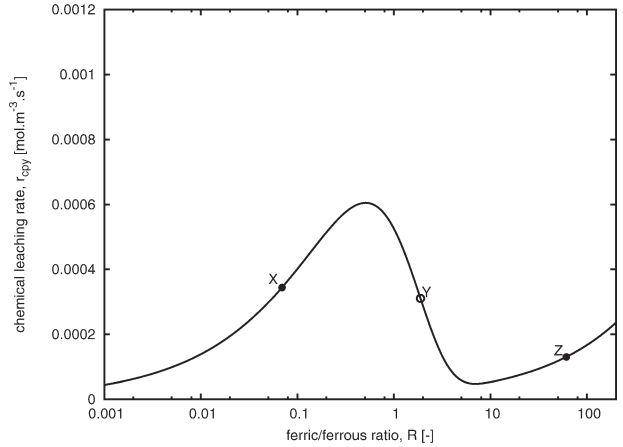

(b)

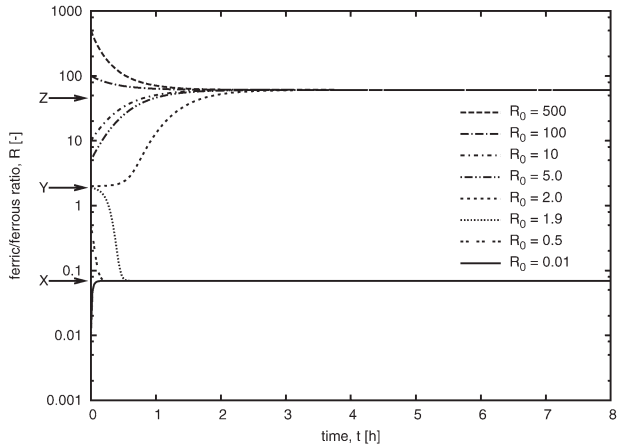

(c)

Figure 4. The dynamics of chalcopyrite indicating multiple steady states *X*, *Y*, and *Z* (*R* = [Fe^{3+}]/[Fe^{2+}]).

When plotting the leaching rate and the microbial oxidation rate in Figure 4a using leaching rate constants $A = 1.40 \times 10^{-3}$ mol m^{-3} s^{-1}, $B = 1.67 \times 10^{-5}$ mol m^{-3} s^{-1}, and $R_{crit} = 1$, and microbial oxidation rate constants $C_X q^{max}_{Fe^{2+}} = 1.40 \times 10^{-3}$ mol m^{-3} s^{-1} and $K = 0.019$, it is clear from Figures 4a, b that a maximum number of three steady states may occur during chalcopyrite bioleaching. During microbial oxidation (Eq. 2), ferrous ions are converted to the ferric form, increasing the ferric/ferrous ion ratio, whereas ferric ions are converted to ferrous ions during chemical leaching, decreasing the redox potential (Eq. 1). Therefore, any region in Figure 4 in which the microbial oxidation rate curve lies above the chemical oxidation rate, the overall reaction shifts to higher redox potentials and vice versa when chemical leaching exceeds microbial oxidation. A stable steady state therefore exists at the intersection of the two rate curves at low solution potentials and another at high solution potentials where microbial oxidation is the dominating reaction (points *X* and *Z* in Figure 4). An unstable steady exists at the intermediate potential region (point *Y* in Figure 4) as potentials to the left or right of this intersection, respectively, result in dominant chemical or microbial oxidation rates, which drive the system away from this point to the lower or higher stable steady-state points *X* and *Z*, respectively. A maximum of two stable steady states *X* and *Z* and one unstable steady state *Y* are therefore observed in chalcopyrite bioleaching.

The time profile for the ferric/ferrous ion ratio *R* is determined by integrating Eq. 9 and plotted in Figure 4c, which confirms graphically that only two stable steady states are achieved in chalcopyrite bioleaching, with an unstable steady state at the intermediate solution potential *Y*.

In attempting to exploit the dynamics for achieving and maintaining high leaching rates, the biomass concentration C_X, which directly affects the microbial oxidation rate (Eq. 4), was varied. The results are shown in Figure 5 as curves L_1, L_2, and L_3. Lines L_1 and L_3 intersect with the leaching rate curve only once, indicating that single steady states with low leaching rates occur before and after the zone of multiple intersections to which L_2 belongs. As these intersecting points determine the stability of operation, they must be identified to avoid low bioleaching rates.

A single steady state exists at intersecting points R_a and R_b in Figures 6a, b. Between these points, there are two stable and one unstable steady state (L_2 in Figure 5). Points R_a

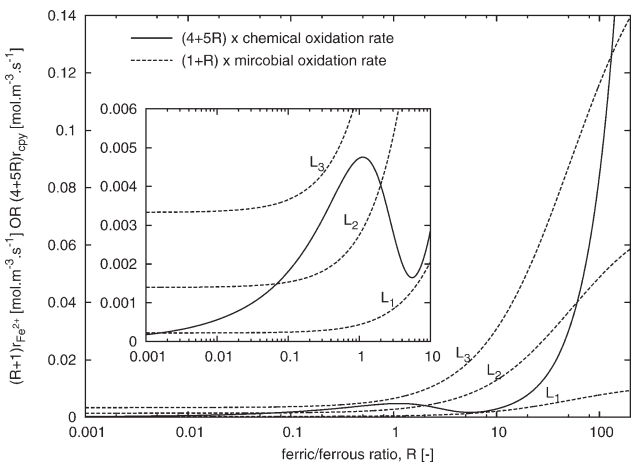

Figure 5. Single steady-state points occur before and after multiple points of stability. Low bioleaching rates occur when one intersection point is observed.

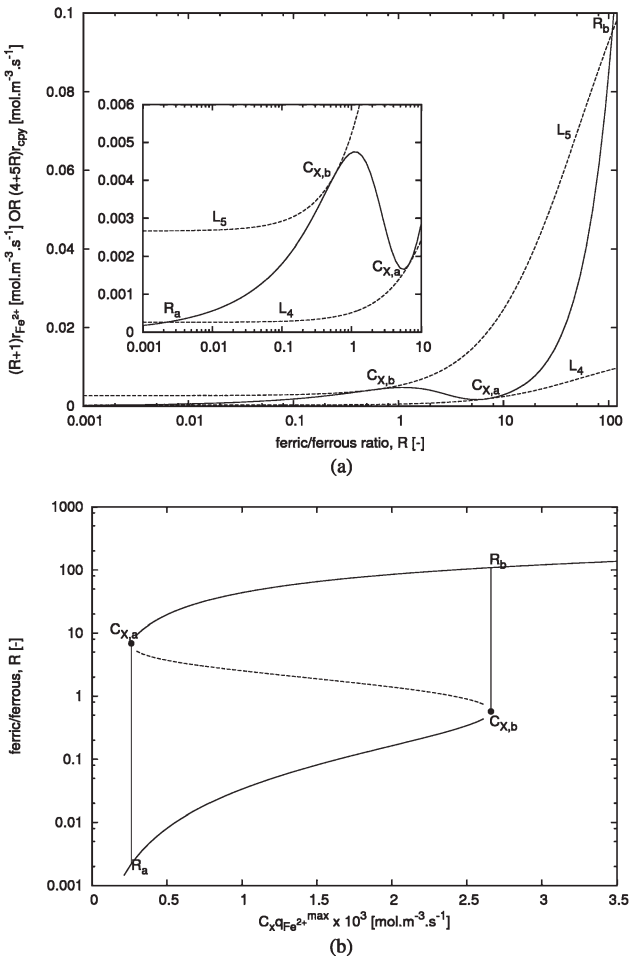

Figure 6. Multiple steady states achieved by varying the biomass concentration C_X.

Points $C_{X,a}$ and $C_{X,b}$ indicate points of tangency of the chemical oxidation rate with the microbial oxidation rate. The solid curves in the phase plane represent stable steady states and the dotted curve unstable steady states.

and R_b are therefore bifurcation points. Geometrically, these bifurcation points occur when the microbial oxidation curve is tangent to the chemical leaching rate curve (L_4 and L_5 in Figure 6a). Mathematically, redox potentials at bifurcation biomass concentrations $C_{X,a}$ and $C_{X,b}$ in Figures 6a, b are obtained when the values of rate functions $(R + 1)r_{Fe^{2+}}$ and $(5R + 4)r_{cpy}$, as well as their gradients with respect to R, are equal (Eqs. 10 and 15, respectively).

$$\frac{d[(5R+4)\cdot r_{cpy}]}{dR} = \frac{d[(R+1)\cdot r_{Fe^{2+}}]}{dR}. \tag{15}$$

When both conditions are satisfied, the rate functions are equal and tangent to each other at the corresponding steady-state points $C_{X,a}$ and $C_{X,a}$.

It is important to note that $C_X q^{max}_{Fe^{2+}}$ and hence the dynamic structure may change during the operation of even a single-batch reactor during a single run, since, as the reaction proceeds, the microbial concentration C_X increases with the generation of ferrous ion substrate during chemical leaching.

If the bioleach reactor operates at any concentration below the bifurcation biomass concentration $C_{X,a}$ (L_4 in Figure 6a), chemical leaching becomes the dominating reaction. The ferric ions in solution are converted to the ferrous form, thus causing the solution potential to drop until the steady state at point R_a is achieved (Figure 6b). Alternatively, if the biomass concentration increases beyond bifurcation point $C_{X,b}$ (L_5 in Figure 6a), the dominant microbial oxidation reaction converts the ferrous ions back to ferric ions, increasing the solution potential until balance is achieved at point R_b. If, in this dynamic study, the rate of chemical leaching coincides with the rate of microbial oxidation at redox potentials between bifurcation biomass concentrations $C_{X,b} < C_X < C_{X,a}$ as in L_2 in Figure 5, the system would be in an unstable steady-state region favoring either ferric or ferrous iron production very close to these points. A slight increase or decrease in the solution potential would result in either the rate of microbial oxidation or chemical leaching becoming dominant and thus shifting the balance to higher or lower stable steady states, respectively. Stable operation at solution potentials between $C_{X,b} < C_X < C_{X,a}$ can only occur if the solution potential is maintained precisely at the intersection potential. As the bifurcation biomass concentrations $C_{X,a}$ and $C_{X,b}$ have been identified, it is now possible to control the system into the maximum operating region by investigating the influence of temperature and biomass concentration on the dynamics.

The influence of temperature on system dynamics

Increased bioleaching rates have been observed with increased operating temperatures. As the chemical leaching and microbial oxidation rates each have different temperature dependencies, the points of steady-state operation may change with temperature. The temperature dependence of the chemical leaching and microbial oxidation rates is therefore established here.

The temperature dependence for the chemical leaching rate is first considered. The chemical leaching of chalcopyrite and its dependence on temperature was extensively studied by Kametani and Aoki.[18] Reasonable fits to this data are obtained by applying the proposed empirical rate expression in Eq. 14[15] (Figure 7). In the absence of a published temperature relationship for the parameters A and B (mol m^{-3} s^{-1}) in Eq. 14, it is proposed that the Arrhenius dependency be adopted in this study.

The rate fits obtained for the leaching of chalcopyrite over a temperature and redox potential range between 298.15 and 363.15 K and 0.30 and 0.65 V (Saturated Calomel Electrode, SCE), respectively, were used to obtain the Arrhenius terms in Eqs. 16 and 17 for the kinetic constants A and B (mol m^{-3} s^{-1}) for the chemical leaching rate in Eq. 14. The Arrhenius fits to this data are graphically represented in Figure 8.

$$A = 1.40 \times 10^{11} e^{\frac{-9.22\times10^4}{RT}} \tag{16}$$

$$B = 1.72 \times 10^{11} e^{\frac{-1.04\times10^5}{RT}}. \tag{17}$$

Next, the temperature dependence for the microbial oxidation rate was also developed. Searby[20] investigated the

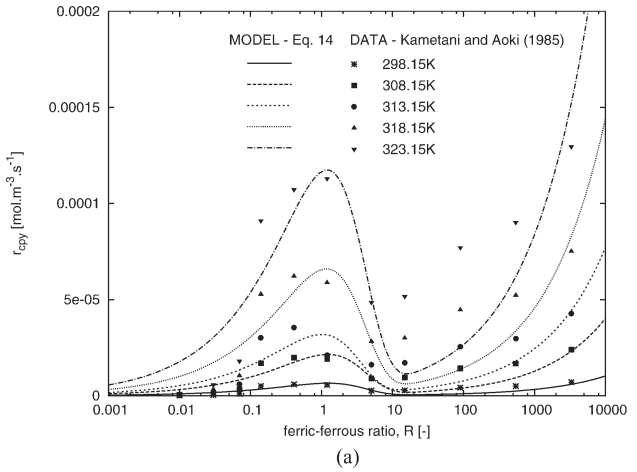

(a)

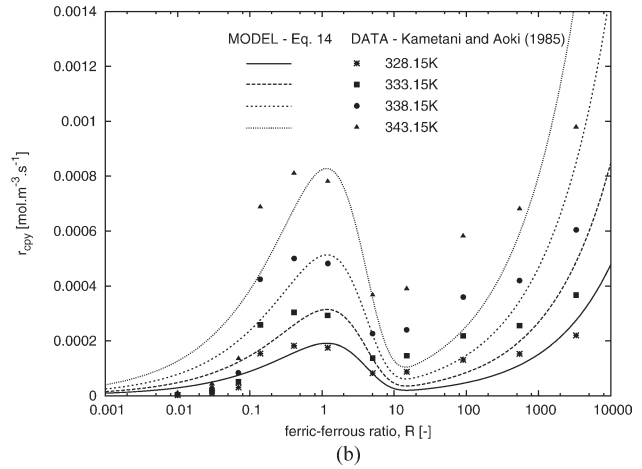

(b)

Figure 7. Validation of the empirical leaching rate proposed by Petersen and Dixon.[15]

Data extracted from Kametani and Aoki[18] and Jaffer.[21]

influence of temperature on the maximum specific iron utilization rate $q^{\max}_{Fe^{2+}}$, and hence the microbial oxidation rate, for a *Metallosphaera* culture between 333.15 and 353.15K. The results indicated that the dependence of $q^{\max}_{Fe^{2+}}$ on temperature was Arrhenius (see Eq. 18).

$$q^{\max}_{Fe^{2+}} = q_0 e^{\frac{-E_a}{RgT}}, \tag{18}$$

where $q_0 = 6.17 \times 10^4$ mol Fe^{2+} mol^{-1} carbon s^{-1} and $E_a = 48.0 \times 10^3$ J mol^{-1}.[20] This then establishes the temperature dependence for the biooxidation rate.

It is evident from the literature that increasing the operating temperature will increase the rate of chalcopyrite bioleaching. If it is assumed that cell growth inhibition at elevated temperatures resulting from mechanical stresses is negligible, the rate dependencies on temperature established from the Arrhenius terms in Eqs. 16–18 for the corresponding rate Eqs. 4 and 14 completely describe the system sensitivity to temperature, making it possible to investigate the effect of temperature on system dynamics.

For the sake of illustration, three operating temperatures of 333.15, 343.15, and 353.15 K at constant biomass concentration were simulated. Figure 9a indicates the change in steady states resulting from the intersection of the chemical leaching rate with the microbial oxidation rate functions $(5R + 4)r_{cpy}$ and $(R + 1)r_{Fe^{2+}}$, respectively. To clearly show the effect of temperature on the chalcopyrite leaching rate, the stable steady-state points are plotted with the chalcopyrite leaching rate in Figure 9b. It is apparent from Figure 9 that both the rates of chemical leaching and microbial oxidation increase with temperature in such a way that the steady-state solution ferric/ferrous ion ratio decreases (Figure 10).

The local maximum of the chemical leaching rate curve increases with temperature, thus increasing the operating region at which stable steady states occur at low redox potentials. The system thus moves from a single stable steady state at low leaching rates, at high solution potentials at 333.15 K (Figure 9b), to two stable steady states at 343.15 and 353.15 K (Figures 9 and 10). For the same given overall biomass concentration, at lower temperatures, the system therefore falls to low rates at lower biomass concentrations than if the system was operated at elevated temperatures (Figure 9b).

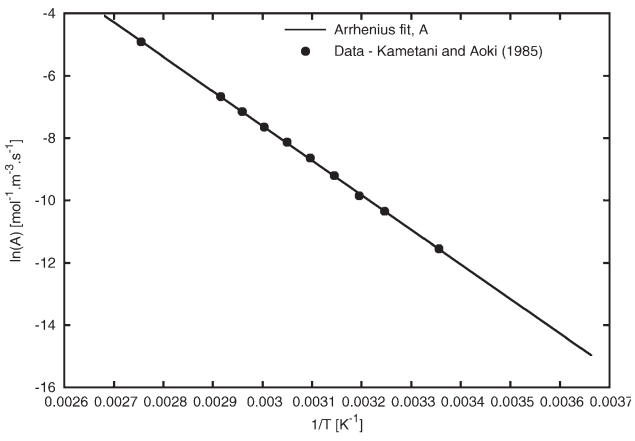

(a)

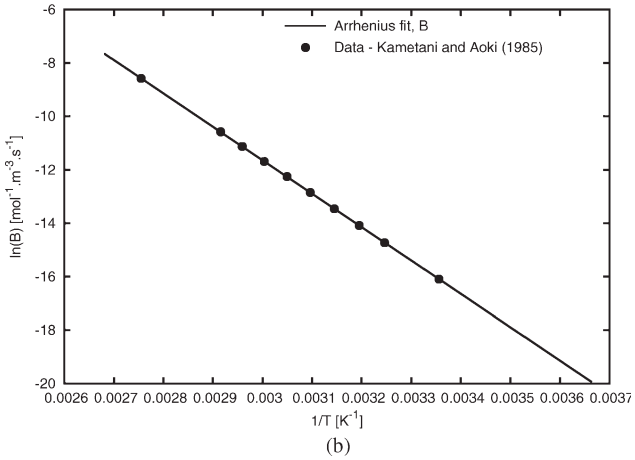

(b)

Figure 8. The effect of temperature on the kinetic constants *A* and *B* in the chemical oxidation rate of chalcopyrite in Eq. 14.

Data reworked from Kametani and Aoki[18] and Jaffer.[21]

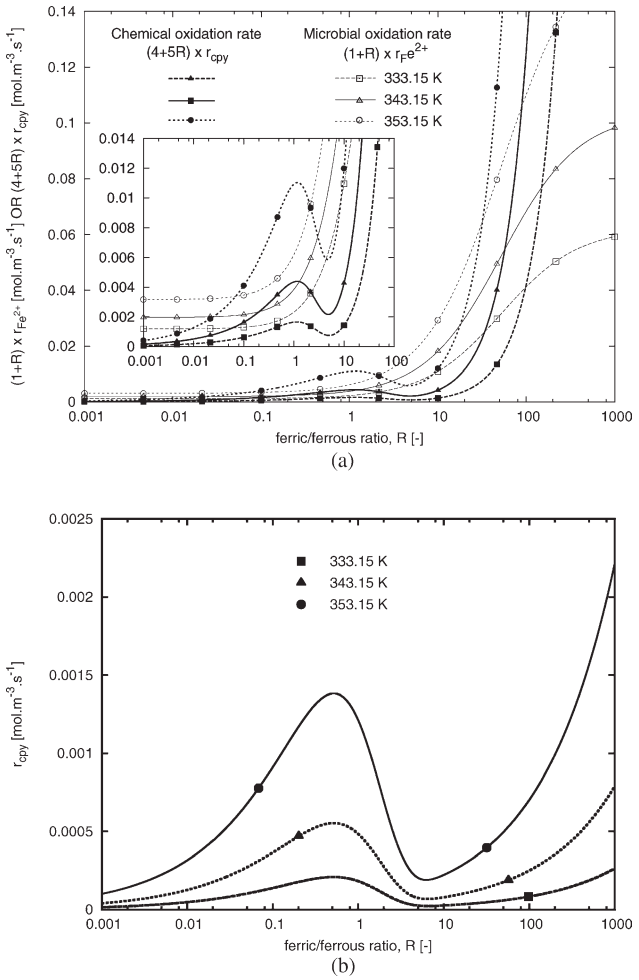

Figure 9. The effect of temperature on the points of stability and the solution ferric/ferrous ion ratio.

The influence of temperature on system steady state is shown in Figure 10. Given that thermal stress influences biomass activity, a feasible limit of 353.15 K does exist, as indicated in the Figure. Temperatures beyond this limit indicate a theoretical representation of the system steady states if the thermophiles were active, and the kinetics were valid at the given temperatures. It appears that by increasing the system temperature, low bioleaching rates at solution potentials beyond 0.65 V (Standard Hydrogen Electrode, SHE) can be overcome with rates comparable to those achieved at low ferric/ferrous ion ratios. However, bioleaching rates at these temperatures depend on the activity of the microorganisms at such high redox potentials.

The influence of biomass concentration on system dynamics

As the rate of microbial oxidation is directly proportional to the concentration of biomass (Eq. 4), an increase in the biomass concentration, at constant temperature, would therefore increase the rate of microbial oxidation without affecting the leaching rate directly and hence, increase the overall bioleaching rate in the system. Graphically, this increase is indicated by an upward shift in the microbial oxidation rate curve with biomass.

For the sake of illustration, three biomass concentrations of 0.5, 0.75, and 1.0 mol carbon m^{-3} were simulated at a constant temperature of 343.15 K. As expected, increased bioleaching rates are observed in Figure 11 with increased biomass concentration. The points of operation shift from multiple steady states to a single stable steady state, indicating that a bifurcation concentration exists prior to low overall bioleaching rates (Figure 6b).

Increasing the biomass concentration shifted the microbial oxidation rate curve such that the initial availability of multiple steady states was reduced to a single stable steady state at higher redox potentials with lower overall bioleaching rates (Figure 11b). It therefore appears that higher leaching rates cannot be achieved by simply increasing the biomass concentration without bound. The leaching rate does increase at low solution potentials until the microbial oxidation rate is tangent to the chemical leaching rate. Up to this point, two stable steady states are observed, one at low solution potentials with high rates and another at high ferric/ferrous ion ratios with low overall bioleaching rates. When the tangent point is exceeded ($C_{X,b}$ in Figure 6b), by increasing the biomass concentration, low rates are observed (Figure 11b). The point of contention in several studies is whether the presence of microorganisms or the addition of ferrous ions increases the rate of leaching.[2–4] The analysis reveals that it is the extent to which the biomass concentration shifts the microbial oxidation rate curve with respect to the leaching rate curve. The addition of ferrous ions to the system would only be beneficial if the bioleach reactor operates at high solution potentials where low rates are observed or once the microbial oxidation rate has exceeded the rate of chemical leaching beyond the bifurcation biomass concentration $C_{X,b}$ (Figure 6b).

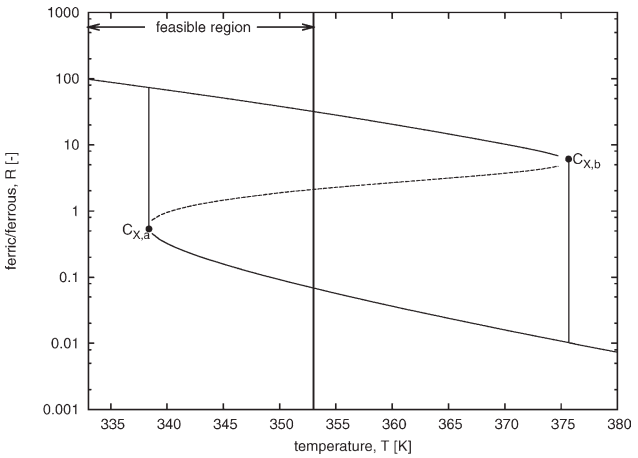

Figure 10. The influence of temperature on the points of stability in a bioleach system.

Points $C_{X,a}$ and $C_{X,b}$ indicate points of tangency of the chemical oxidation rate with the microbial oxidation rate. The solid curves in the phase plane represent stable steady states and the dotted curve unstable steady states. The solid vertical separator indicates the maximum feasible temperature 353.15 K for the thermophiles investigated by Searby.[20]

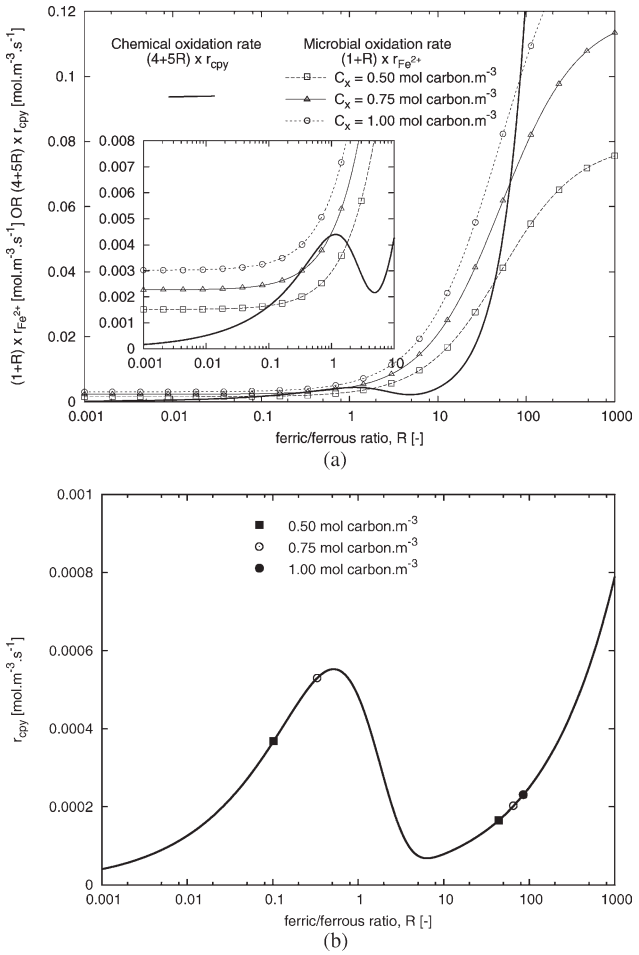

Figure 11. The influence of biomass concentration on the points of stability and the solution ferric/ferrous ion ratio.

Without a dynamics analysis, it would never be clear which kinetic consideration is causing the behavior considered, therefore without it, the reports will always appear to be in conflict. The biomass concentration is therefore an important parameter that should be monitored to prevent low overall bioleaching rates.

The combined influence of temperature and biomass on system dynamics

In both temperature and biomass case studies, it emerged that higher leaching rates could be achieved at higher solution potentials by either increasing the system temperature or increasing the biomass concentration.

If Eqs. 10 and 15 are simultaneously solved at steady state for a range of temperatures with corresponding biomass concentrations, the locus of tangent points, $C_{X,a}$ and $C_{X,b}$, can be obtained (Figure 12) from which the optimal operating region can be easily predicted. Multiple steady states are achievable between the locus of tangents $C_{X,a}$ and $C_{X,b}$. The stable operating region increases with temperature and biomass concentration increasing the overall bioleaching rate. Any operating point below or above $C_{X,a}$ and $C_{X,b}$ in Figure 12, respectively, would result in diminished rates, although at higher temperatures and biomass concentrations competitive rates are possible at high redox potentials (Figures 9 and 11).

Experimental Validation

Third et al.[1] focused on the role of microorganisms in the bioleaching of chalcopyrite. By studying the effects of different inoculum sizes, these researchers reported that bioleaching rates appeared to fall to different extrema when a range of inoculum volumes were introduced to their bioleaching experiments, thus indicating the presence of more than one steady state (Figure 13). The authors hypothesized that the bioleaching rate was not only dependent on the microbial concentration or activity but is also largely dependent on the initial solution redox potential.[1] However, this was the limit of their explanation for this observation, which was largely regarded as an anomaly that did not correspond to the established theoretical frameworks. However, by application of the dynamic analysis introduced in this article, we are able to predict both sets of extrema within one unified model (Figure 13).

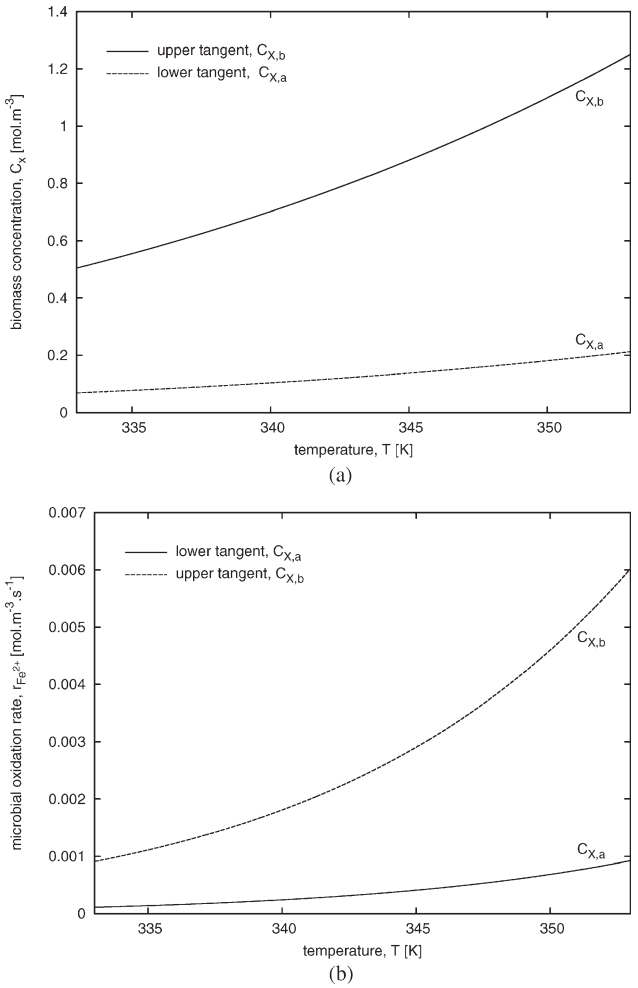

Figure 12. Locus of tangent points $C_{X,a}$ and $C_{X,b}$ as a function of temperature and biomass concentration.

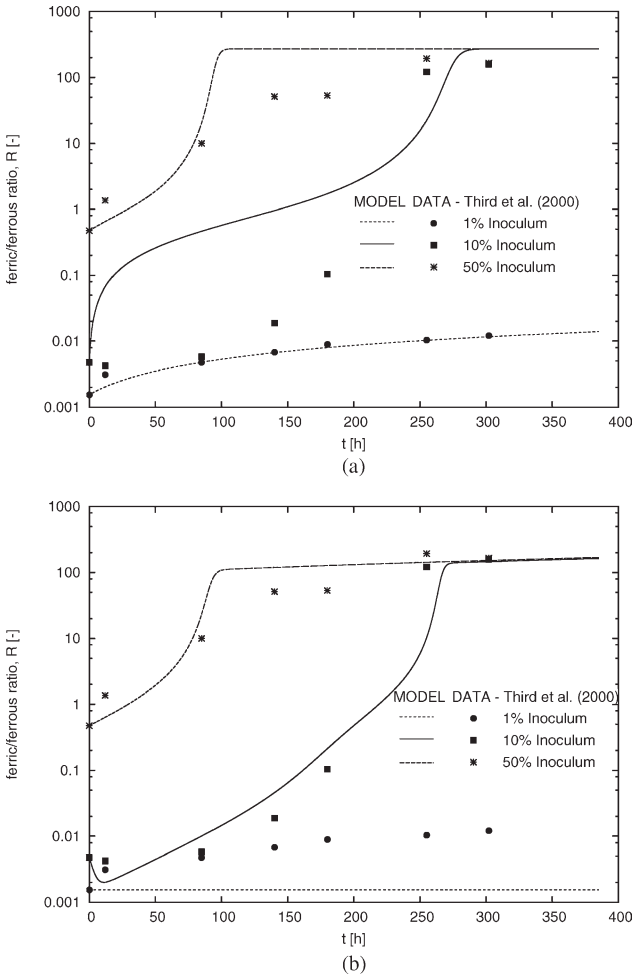

Figure 13. Dynamic model validation against chalcopyrite bioleaching data extracted from Third et al.[1]

The leaching rate constants A, B, R_c, the microbial rate constants $q^{max}_{Fe^{2+}}$, K, and the final microbial concentration C_x are unknown for these experiments and are therefore used as the fitting parameters when validating the model with the data.

Two approaches were adopted when applying the dynamics analysis to this experimental data. The first analysis incorporated material balances for the redox potential and the ferrous ion concentration, whereas the second analysis incorporated a material balance for the biomass. In the latter case, the biomass was assumed to exhibit growth, inhibition, and death. The latter was modeled as a first-order reaction rate, in which case the additional parameter k_d was fit from the data.

In Figure 13a, it is shown that in analysis 1 (which does not include a material balance for the biomass concentration), the best parameter fits gave leaching rate constants $A = 6.38 \times 10^{-4}$ kg m^{-3} s^{-1}, $B = 3.62 \times 10^{-7}$ kg m^{-3} s^{-1}, $R_c = 0.86$ and microbial rate constants $q^{max}_{Fe^{2+}} = 0.0028$ mol Fe^{2+} mol carbon^{-1} s^{-1}, $K = 0.027$. At these values, we are able to predict the observed multiple steady states for initial inoculum sizes 1% (v/v) and 50% (v/v) at low and high solution redox potentials, respectively, as well as the transition from fast to slow bioleaching rates observed when a 10% (v/v) inoculum was used. The maximum microbial specific ferrous iron utilization rate $q^{max}_{Fe^{2+}}$ and inhibition constant K predicted by the model for the mixed mesophilic culture used by Third et al.[1] compares favorably with those reported for pure cultures *Leptospirillum ferrooxidans* $q^{max}_{Fe^{2+}} = 0.0019$ mol Fe^{2+} mol carbon^{-1} s^{-1}, $K = 0.0005$ and *Acidothiobacillus ferrooxidans* $q^{max}_{Fe^{2+}} = 0.0024$ mol Fe^{2+} mol carbon^{-1} s^{-1}, $K = 0.05$.[16]

The second analysis (including biomass balance) yields a slightly better fit for the 10% (v/v) inoculum (Figure 13b). However, the steady state at the lower ferric/ferrous ion ratio was not accurately predicted, and the regressed rate constants $q^{max}_{Fe^{2+}} = 1.0 \times 10^{-4}$ mol Fe^{2+} mol carbon^{-1} s^{-1}, $K = 0.033$ for the microbial oxidation rate were not comparable with those reported in literature. Therefore, the rate constants obtained during the first analysis were adopted for the dynamics analysis that follows.

From the chalcopyrite rate curves in Figure 14, it is shown that the predicted microbial oxidation rate at low solution potentials and microbial concentration exceeds the chalcopyrite leaching rate. The reaction is thus driven to higher solution potentials with microbial growth. On the other hand, the 1% (v/v) inoculum data shown in Figure 14a reveal fast bioleaching rates are achieved when the redox potential remains below the redox potential at bifurcation biomass concentration $C_{X,b}$, $R = 0.54$. As ferrous ions are not actively converted to ferric ions and there was no noticeable microbial growth at these conditions, the system remains at the low ferric/ferrous ion ratio range where fast bioleaching rates X are observed.

Similarly, in the 50% (v/v) inoculum experiment, low rates are observed at high ferric/ferrous ion ratios, beyond the bifurcation biomass concentration $C_{X,a}$, $R = 5.62$, as predicted by the model (Figure 14c). Because of the high initial redox potential combined with a large initial inoculum size, the system immediately falls to slow overall rates Z_0. The system will therefore never attain fast bioleaching rates as the microbial oxidation rate only intersects the chemical leaching rate once at ferric/ferrous ion ratios beyond the bifurcation biomass concentration $C_{X,a}$.

Third et al.[1] noted that with the 10% (v/v) inoculum experiment, the copper leaching rate was fast when microbial activity was low. With microbial growth, and hence an increase in the ferric/ferrous ion ratio, the bioleaching rate moved from fast to slow bioleaching rates when 10% (v/v) inoculum was introduced to the experiment at low solution potentials. At the given conditions, it can be seen in Figure 14b that the microbial oxidation rate curve intersects the chemical leaching rate curve thrice, with stable steady states observed at low X_0 and high Y_0 ferric/ferrous ion ratios. With increased microbial activity and hence growth, ferrous ions are converted to ferric ions, thereby increasing the ferric/ferrous ion ratio. Bioleaching rates therefore move from fast X_0 to slow Z overall rates because of the change in the solution potential and microbial concentration. It is also noted in Figure 14b that with microbial growth, there is a transition from two possible stable steady states X_0 and Z_0, when three intersections are observed, to a single stable steady state Z when the microbial oxidation rate curve intersects the chemical leaching rate curve once, at high ferric/ferrous ion ratios. This transition from multiple X_0, Z_0 to single Z stable steady states verifies that a critical microbial concentration exists before system inhibition (Figure 14b).

In summary, the dynamic analysis shows that the overall rate is inhibited when a certain critical microbial concentration and solution potential are exceeded. Analysis of the experimental data and model indicated that the microbial concentration can be both beneficial and detrimental to the overall bioleaching process and is largely dependent on the initial redox potential. In light of these analyses, the existing experimental observations such as those by Third et al.[1] can now be understood and brought within a single unified theoretical framework.

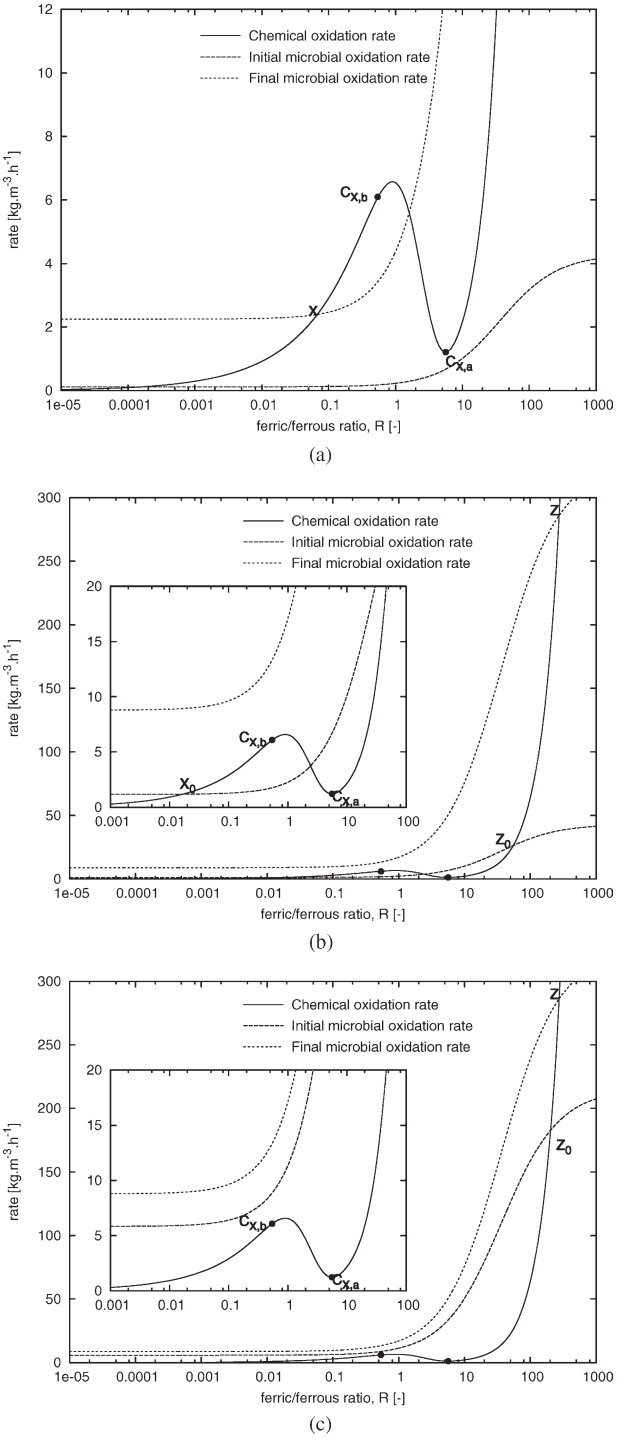

Figure 14. Predicted microbial and leaching rates for experimental data extracted from Third et al.[1]

Annotations *X* and *Z* indicate stable steady states at low and high ferric/ferrous ion ratios, respectively.

Table 1. Assumed Parameters for the Chemical and Microbial Oxidation Rates in Figure 2

Chemical Oxidation Rate Constants		Microbial Oxidation Constants	
K (mol m^{-3} s^{-1})	n	$C_X q^{max}_{Fe^{2+}}$ (mol m^{-3} s^{-1})	K
3.5×10^{-8}	0.5	1.2×10^{-5}	5×10^{-3}

Conclusions

Because of the nonmonotonic relationship between the chalcopyrite leaching rate and solution potential, a dynamics analysis was conducted to determine important operational features for the batch processes. This study has shown that two stable steady states are possible at low and high redox potentials with one unstable steady state at intermediate ferric/ferrous ion ratios. High leaching rates are observed at redox potentials below 0.65 V (SHE), whereas low rates are observed at high potentials. In general, it was found that the overall bioleaching rate is sensitive to the solution redox potential, system temperature, and biomass concentration.

A method for determining optimal operation for given biomass concentration and temperatures was proposed. Using this technique, the domains of steady states and their stability with respect to the operating variables, viz., temperature and biomass concentration, were used to identify regions of operation. This study indicates that if both the system temperature and the biomass concentration are increased within the defined feasible region, increased bioleaching rates can be recognized at high redox potentials. To verify whether the theoretical phenomena outlined in this study do occur in reality, the analysis was applied to experimental data.

Application of the dynamic analysis outlined in this article to experimental data obtained from Third et al.[1] proved that the model is able to accurately predict the observed steady states at low and high ferric/ferrous ion ratios. A dynamics analysis of the data verified the existence of multiple steady states in chalcopyrite bioleaching, and that overall rates are sensitive to the combination of the ferric/ferrous ion ratio with the biomass concentration and system temperature.

These results show that observed low rates of chalcopyrite bioleaching traditionally explained by the formation of a passivating layer on the mineral particle surface or the susceptibility of the biomass cell structure to mechanical stress at elevated temperatures are in fact simply artifacts of the dynamics of chalcopyrite bioleaching, and the many reports about the influence of these parameters on the bioleaching rate must be subjected to a rigorous dynamics analysis to integrate them into a consistent understanding of the underlying kinetics.

Acknowledgments

This work was carried out in the frame of BioMinE (European project contract NMP1-CT-500329-1). The authors acknowledge the financial support given to this project by the European Commission under the

Sixth Framework Program for Research and Development. The authors also thank their various partners on the project for their contributions to the work reported in this article.

Notation

Greek letters

α = stoichiometric coefficient of the ferric ions in solution according the chemical leaching reaction
β = stoichiometric coefficient of the ferrous ions in solution according the chemical leaching reaction

Latin letters

A^{p} = particle specific surface area ($m^2\ m^{-3}$)
A = temperature-dependent rate constant for the chemical leaching of chalcopyrite (mol $m^{-3}\ s^{-1}$)
B = temperature-dependent rate constant for the chemical leaching of chalcopyrite (mol $m^{-3}\ s^{-1}$)
$C_{\mathrm{Fe^{3+}}}$ = concentration of ferric ions (mol m^{-3})
$C_{\mathrm{Fe^{2+}}}$ = concentration of ferrous ions (mol m^{-3})
C_{X} = concentration of the biomass (mol carbon m^{-3})
$C_{\mathrm{X,a}}$ = bifurcation biomass concentration at high ferric/ferrous ion ratios (mol carbon m^{-3})
$C_{\mathrm{X,b}}$ = bifurcation biomass concentrations at low ferric/ferrous ion ratios (mol carbon m^{-3})
E_{a} = activation energy (kJ mol^{-1})
$f(X_{\mathrm{cpy}})$ = topological term
g_{py} = mineral grade
K = inhibition constant
k = intrinsic rate constant (mol $m^{-2}\ s^{-1}$)
k_{d} = death rate kinetic constant (s^{-1})
n = reaction order
$q^{\max}_{\mathrm{Fe^{2+}}}$ = maximum microbial-specific ferrous iron utilization rate (mol Fe^{2+} mol^{-1} carbon s^{-1})
q_0 = maximum microbial-specific ferrous iron utilization rate at the reference temperature T (mol Fe^{2+} mol^{-1} carbon s^{-1})
R = ferric/ferrous iron ratio ($R = [Fe^{3+}]/[Fe^{2+}]$)
R_{a} = bifurcation point at high ferric/ferrous ion ratios
R_{b} = bifurcation point at low ferric/ferrous ion ratios
R_{g} = universal gas constant (J $mol^{-1}\ K^{-1}$)
r_{cpy} = intrinsic chemical leaching rate for chalcopyrite (mol $m^{-3}\ s^{-1}$)
$-r_{\mathrm{Fe^{2+}}}$ = microbial oxidation rate (mol $m^{-3}\ s^{-1}$)
r''_{MS} = intrinsic rate for most mineral sulfides MS (mol $m^{-2}\ s^{-1}$)
T = temperature (K)
t = time (s)

Literature Cited

1. Third KA, Cord-Ruwisch R, Watling HR. The role of iron-oxidizing bacteria in stimulation inhibition of chalcopyrite bioleaching. *Hydrometallurgy*. 2000;57:225–233.
2. Hiroyoshi N, Miki H, Hirajima T, Tsunekawa M. Enhancement of chalcopyrite leaching by ferrous ions in acidic ferric sulfate solutions. *Hydrometallurgy*. 2001;60:185–197.
3. Dutrizac JE, MacDonald RJC, Ingraham TR. The kinetics of dissolution of synthetic chalcopyrite in aqueous acidic ferric sulfate solutions. *Trans Metall Soc AIME*. 1969;245:955–959.
4. Hirato T, Majima H, Awakura Y. The leaching of chalcopyrite with ferric sulfate. *Metall Trans B*. 1987;18:489–496.
5. Clark DA, Norris PR. Oxidation of mineral sulphides by thermophilic microorganisms. *Miner Eng*. 1996;9:1119–1125.
6. Nemati M, Harrison STL. Effect of solid loading on thermophilic bioleaching of sulfide minerals. *J Chem Technol Biotechnol*. 2000;75:526–532.
7. Sissing A, Harrison STL. Thermophilic mineral bioleaching performance: a compromise between maximizing mineral loading and maximizing microbial growth and activity. *J S Afr Inst Min Metall*. 2003;103:139–142.
8. Witne JY, Phillips CV. Bioleaching of 0K Tedi copper concentrate in oxygen-and carbon dioxide-enriched air. *Miner Eng*. 2001;14:25–48.
9. Valencia P, Gentina JC, Acevedo F. Effect of pulp density and particle size on the biooxidation rate of a pyritic gold concentrate by *Sulfolobus metallicus*. In: *Proceedings of the International Biohydrometallurgy Symposium*, Athens, Greece, 2003.
10. Bailey AD, Hansford GS. Oxygen mass transfer limitation of batch bio-oxidation at high solids concentration. *Miner Eng*. 1994;7:293–303.
11. Loia G, Mura A, Trois R, Rossi G. Bioreactor performance versus solids concentration in coal biodepyritization. *Fuel Process Technol*. 1994;40:251–260.
12. Kotsiopoulos A, Hansford GS, Rawatlal R. An approach of segregation in modeling continuous flow tank bioleach systems. *AIChE*. 2008;54:1592–1599.
13. Breed AW, Hansford GS. Modeling continuous bioleach reactors. *Biotechnol Bioeng*. 1999;64:671–677.
14. Boon M, Heijnen JJ. Chemical oxidation kinetics of pyrite in bioleaching processes. *Hydrometallurgy*. 1998;48:27–41.
15. Petersen J, Dixon DG. Competitive bioleaching of pyrite and chalcopyrite. *Hydrometallurgy*. 2006;83:40–49.
16. Hansford GS. *Recent developments in modelling the kinetics of bioleaching*. In: Rawlings DE, editor. *Biomining: Theory, Microbes and Industrial Processes*. Berlin: Springer, 1997:153–176.
17. Olson GJ. Rate of pyrite bioleaching by *Thiobacillus ferrooxidans*: results of interlaboratory comparison. *Appl Environ Microbiol*. 1991;57:642–644.
18. Kametani H, Aoki A. Effect of suspension potential on the oxidation rate of copper concentrate in a sulphuric acid solution. *Metal Trans B*. 1985;16:695–705.
19. Hiroyoshi N, Kuroiwa S, Miki H, Tsunekawa M, Hirajima T. Synergistic effect of cupric and ferrous ions on active-passive behavior in anodic dissolution of chalcopyrite in sulfuric acid solutions. *Hydrometallurgy*. 2004;74:103–116.
20. Searby GE. An investigation of the kinetics of thermophilic microbial ferrous iron oxidation in continuous culture. Ph.D. thesis, University of Cape Town, Cape Town, South Africa, 2006.
21. Jaffer A. An investigation into the mechanism of bioleaching of a predominantly-chalcopyrite concentrate with mesophiles. Masters thesis. University of Cape Town, Cape Town, South Africa, 2002.

Manuscript received Feb. 25, 2009, and revision received Nov. 26, 2009.